Modelling Ordered Packed Beds of Spheres: The Importance of Bed Orientation and the Influence of Tortuosity on Dispersion

Elsevier Editorial System(tm) for Journal of Chromatography A

Manuscript Draft

Manuscript Number: JCA-17-1294R2

Title: Modelling Ordered Packed Beds of Spheres: The Importance of Bed Orientation and the Influence of Tortuosity on Dispersion

Article Type: Full length article

Keywords: Ordered packing; Lattice Boltzmann; Chromatographic Efficiency; Permeability; Tortuosity

Corresponding Author: Mr. Fabian Dolamore, Ph.D. (candidate)

Corresponding Author's Institution: University of Canterbury

First Author: Fabian Dolamore, Ph.D. (candidate)

Order of Authors: Fabian Dolamore, Ph.D. (candidate); Conan J Fee, PhD; Simone Dimartino, PhD

Modelling Ordered Packed Beds of Spheres: The Importance of Bed Orientation and the Influence of Tortuosity on Dispersion

Fabian Dolamore[1,2,*], Conan Fee[1,2,3] Simone Dimartino[3,4]

[1] Chemical and Process Engineering, University of Canterbury, Private Bag 4800, Christchurch 8041, New Zealand

[2] Biomolecular Interaction Centre, University of Canterbury

[3] School of Product Design, University of Canterbury

[4] Institute for Bioengineering, School of Engineering, The University of Edinburgh, Edinburgh EH9 3FB, UK

*Corresponding author. email: fabian.dolamore@pg.canterbury.ac.nz; tel: +64(0)27 7282030

Abstract

Ordered packing has previously been considered for porous media applications in the industrial and analytical worlds, with implementation constrained only by the lack of feasible fabrication methods. Additive manufacturing now provides the answer to this limitation, which leads to the novel domain of customized ordered packing and a variety of optimized geometries. In this work, the chromatographic behaviour of ordered configurations of particles was described using computational fluid dynamics methods based on the Lattice Boltzmann Model. The model was first validated by matching van Deemter trends for ordered and random packings shown in previous research. The influence of rotations of the ordered configurations was then considered, indicating that orientational changes with respect to the main flow axis can strongly affect minimum plate height. In particular, it is demonstrated that targeted rotations of ordered packings can reduce axial dispersion while improving transverse dispersion, thus improving chromatographic performance. This principle is clearly shown in a strong linear correlation between tortuosity and plate height, offering an additional parameter to enable *a priori* control of the performance of ordered packings. Furthermore, rotation of the packing does not change porosity or surface area and has a relatively small effect on permeability. Thus, highly permeable packings with poor dispersion can be improved in terms of chromatographic impedance by simple rotation of the packing orientation. This work further demonstrates the advantages of ordered packings over randomly packed beds, and introduces new perspectives on the development of chromatographic structures with improved performance.

1. Introduction

The stationary phase in traditional liquid chromatography columns is composed of randomly packed beads. Packing processes are strongly dictated by manufacturing capability, and variants of slurry packing are almost universally applied in both industrial and analytical column production [1-3]. Until now, slurry packing has been the exclusive method by which chromatography columns are produced, with the resulting disordered packing simply regarded as an unavoidable outcome. However, column-to-column variability is often observed, mainly resulting from the random nature of this fabrication step, thus impacting product consistency [4, 5]. Accordingly, all columns undergo stringent quality control and validation procedures to ensure random packing is free from major defects that would

lead to a number of issues such as channelling, stagnation regions or other non-ideal flow behaviours, which negatively impact chromatographic performance [6].

Schure et al. were the first to challenge the concept of randomly arranged particles, and speculated about the advantages of ordered packings in chromatographic columns [7]. Using the Lattice Boltzmann Method (LBM), they demonstrated that the height equivalent to a theoretical plate (HETP) for a face centred cubic (FCC) packing of spheres was considerably lower than that for randomly packed spheres over a broad range of reduced velocities. There has been only a handful of computational studies since Schure's initial research, e.g. ordered packings of ellipsoidal particles [8, 9] or pillar arrays [10, 11], yet all of these studies have consistently demonstrated that ordered packings have the capability to outperform random arrangements of spherical particles. The tangible improvement in chromatographic performance is mainly related to a reduction in eddy dispersion in ordered packings. Despite the promise of such theoretical results, technical and financial constraints have precluded the manufacture of columns with precisely ordered packings until now.

An imminent paradigm shift in column manufacturing is now offered by additive manufacturing technology (AM, or 3D printing), as it enables the creation of complex geometries with high precision. 3D printing was recently employed by Fee et al. to fabricate perfectly ordered column packings, revolutionizing the design and production of chromatographic stationary phases [12]. Later, Nawada et al. evaluated the performance of 3D printed beds of ordered particles, thus experimentally validating the trends predicted by the above computational studies [13]. The exponential growth we are currently witnessing in the 3D printing arena indicates that AM methods with improved resolution, reduced printing times, and enlarged build sizes will soon be available, making the printing of chromatographic stationary phases a reality at industrial scale. Clearly, AM now provides a completely new context for computational studies of perfectly ordered column configurations. Computational Fluid Dynamics (CFD) applied to hypothetical arrangements of particles is no longer an academic speculation but rather offers a predictive tool to help identify suitable geometries for chromatographic operations in a time and cost-efficient manner [14]. Identical geometries can later be fabricated using AM tools to finally obtain physical replicas of improved chromatographic packings.

Among the CFD methods currently available, the LBM is currently preferred when modelling complex geometries such as porous media [7, 10, 11, 15]. The LBM efficiently handles a high proportion of fluid/solid boundaries in the simulation domain, allowing the generation of accurate results in much shorter simulation times than do conventional CFD tools based on the Navier-Stokes equations [16, 17].

The possibilities offered by AM, coupled with the computing capabilities of the LBM, provide a renewed impetus in the exploration of the performance of ordered morphologies of packed beds. In this work, we employed a new approach for the LBM to measure *in silico* column metrics such as HETP, pressure drop and tortuosity. This approach was first validated against prior research results for random and ordered sphere packings. Different configurations for ordered packings were then considered, including various packing arrangements and relative orientations with respect to the main direction of flow. This report highlights, for the first time, key aspects that should be taken into account when designing new ordered morphologies for packed bed columns. For example, we propose the use of flow tortuosity of the porous lattice (based upon the fluid phase velocities) as an indicator of column performance. Such observations will help direct CFD investigations towards

higher performing morphologies that can be potentially fabricated through AM and experimentally tested.

2. Theory and Description of Computational Methods

2.1. *Hardware & Software*

Simulations were performed using a variety of parallel computing systems. The largest simulations were performed using 1024 nodes of an IBM Blue Gene/P (IBM, NY, USA) (four cores running in virtual node mode), while smaller simulations used two nodes of a Power 755 cluster (IBM, NY, USA) (32 cores per node). These systems were both operated under the New Zealand eScience Infrastructure (NeSI).

Palabos (FlowKit Ltd., Lausanne, Switzerland), an open source C++ library, was selected to solve the mathematical framework of the LBM. Palabos is fully parallelized and thus extremely efficient on cluster computing [18]. A front-end script was prepared to use the Palabos library, generate the domain and solve the system's governing equations. Flow field data from simulations were stored in visualization toolkit (.vtk) files and post-processed using Paraview (Kitware Inc., NY, USA), while data from the advection-diffusion process were written to text files (.txt) and analysed using spreadsheets designed to calculate the appropriate performance metrics (Section 2.5).

2.2. Lattice Boltzmann Method

To simulate fluid flow and dispersion in the mobile phase of the domain, the LBM was used. The LBM is a method that has been the subject of rapid development in the last decade because of its suitability for simulating complex geometry flow fields, such as those in porous media [16, 17, 19].

This approach considers a fluid as a collection of particles, unlike the standard Navier-Stokes approach, which considers a fluid body as a continuum. The LBM uses a probability density function (PDF) to convert the discrete particle system into a continuous variable, which is subsequently discretized into a homogenous grid to perform the numerical iterative solution procedure. Macroscopic variables may then be calculated as moments of the PDF. Although the LBM is based on a rarefied gas system, it may be extended to liquid systems by artificially manipulating the Mach number to approach a compressibility limit.

Further details on the LBM parameters used are noted in Section 2.4.

2.3. *Domain and Boundary Conditions*

The domain was spatially discretized using a homogeneous mesh, comprised of 30^3 nodal points per spherical particle (mesh independence study described in Section 3.1). Two superimposed lattices were applied, the first to resolve the steady-state velocity field and the second applied subsequently to resolve the advection-diffusion field.

Both random and ordered packings were considered in this work. All packings were generated from spherical particles with a uniform diameter of 200 µm, i.e. the minimum diameter that can be currently achieved reliably in some commercial 3D printers [20]. The position of each spherical

particle is identified by the location of its centre, which in turn depends upon the packing configuration.

- *Random packings*: an external code was used to generate the centre locations [21] which were imported into Palabos to create the random packings. Five different random packings were generated and employed for the simulations. Packings were $7d_p^3$ in size, where d_p is the sphere diameter. Simulation results were averaged over the five independent packings.
- *Ordered packings*: both particle arrangement and orientation of the packings with respect to the main direction of the flow were considered. Three arrangements, Simple Cubic (SC), Body Centred Cubic (BCC) and Face Centred Cubic (FCC), all based on a cubic unit cell, were generated. The cubic cells were investigated for [001], [011] and [111] orientations, where the main direction of the flow is aligned with the z axis (Fig. 1). The notation in this work uses the Miller Index to denote the axial direction with respect to the standard cubic cell packing. The rotations of the unit cell were produced using rotation matrices on the coordinates of the sphere centres of the standard [001] configuration, a result equivalent to changing the direction of flow with respect to the packing. It is worth noting that, for the same particle diameter, the size of the cubic unit cell as well as the number of particles contained in the unit cell varied amongst the configurations considered (Table 1).

Simulations were run on appropriate multiples of the representative unit cells. A single unit cell was used in the transverse directions (x and y), with periodic boundary conditions applied across all four transverse boundaries. The unit cell was repeated a suitable number times in the axial direction (z), depending on particle arrangement, orientation and axial velocity.

As mentioned above, the simulations involved coupling of two lattices, each requiring specific boundary conditions at the entrance and exit of the domain:

- *Velocity lattice:* a flat velocity profile was defined at the inlet of the domain using a Dirichlet boundary, representative of an ideal and uniform inlet distribution across the entire cross-section of the column. A zero-pressure condition was set at the outlet to generate a pressure gradient along the axial length of the column.
- *Advection-diffusion lattice:* a Dirichlet boundary was used at the inlet to generate a uniform concentration profile, indicative of an ideal and uniform distribution of an inert tracer at the column entrance. The concentration of the tracer at the inlet boundary was manipulated to simulate pulse injections. While pulse injections are mathematically described by the Dirac function, the large concentration gradients arising from this function lead to numerical instabilities in simulation environments [22]. Therefore, a hyperbolic tan function was used to model the inert tracer pulse, providing a smooth and stable, yet physically realistic, pulse of tracer into the column. The outlet was defined as a Neumann boundary, through which the diluted tracer exited the column.

The “bounce-back” condition was imposed at the solid-fluid interface surrounding the spherical particles in both lattices. This corresponds to the no-slip condition in the velocity lattice, while it excludes mass transport inside the particles in the advection-diffusion lattice, thus effectively simulating non-porous beads [23].

All simulated packings had rectangular overall cross-sections to maintain the integrity of the cubic unit cell across the entire column domain. Use of a rectangular geometry does not represent a limitation when the performance of the packing alone (i.e. without walls) is considered, because the behaviour of the unit cell is fully representative of the wider homogeneous packing [7, 10, 11, 15].

The stationary phase was assumed to be rigid, so physical deformation arising from mobile phase flow was neglected.

2.4. Simulation procedure

All simulations used a separate D3Q19 scheme for both the velocity and advection-diffusion lattices. The former used the standard Bhatnagar–Gross–Krook (BGK) collision model [24], while the advection-diffusion lattice used a recently developed, modified single relaxation time (SRT) model [25] to simulate the bulk movement of the solute. This model uses a reference diffusion value to alleviate instabilities, which can arise when solving the advection-diffusion equation using the LBM, by introducing a "diffusion velocity" to the advection term. This method is an alternative to the popular Random Walk Particle Tracking (RWPT) method, which simulates the movement of multiple individual particles in the flow system, usually over multiple runs [7, 26]. In the reference diffusion system, the velocity and concentration fields were coupled, each characterized by the kinematic viscosity of water (ν = 1 x 10^{-6} m^2s^{-1} [27]) and the diffusion coefficient of NaCl (inert tracer) in water (D_m = 2 x 10^{-9} m^2s^{-1} [28]), respectively.

In our approach, the steady state velocity flow fields were first solved and then an idealized pulse of low molecular weight, inert tracer (nominally NaCl) was applied at the column inlet. Accordingly, collision and streaming steps were initialized on the velocity lattice until the system reached steady state. The concentration pulse was then introduced at the inlet of the domain and simulation on the advection-diffusion lattice was commenced. Advection parameters were passed passively from the velocity lattice to the advection-diffusion lattice, assuming that the tracer had negligible effect on fluid properties (density, viscosity) and hence did not affect the velocity profile. The residence time distribution (RTD) curves were determined by monitoring the NaCl concentration downstream over time, conveniently mimicking experimental practice using an inert tracer in real systems. This approach differs from previous studies [7, 10, 11, 15], in which RTDs were constructed from summation of the residence times for individual "particles" generated at various starting points across the column cross-section over multiple runs.

The two key non-dimensional numbers of this problem are the Reynolds (Eq. 1a) and Peclet numbers (Eq. 1b), which are indicative of the regimes present in the flow and in the advection-diffusion lattices, respectively. These two non-dimensional parameters are directly linked by the ratio of the kinematic viscosity of the fluid, ν, and the diffusion coefficient of the solute, D, also known as the Schmidt number (Eq. 1c), which is 500 for the systems investigated in this work.

$$Re = \frac{d_p v_c}{\nu} \qquad (1a)$$

$$Pe = \frac{d_p v_c}{D} \qquad (1b)$$

$$Sc = \frac{Re}{Pe} = \frac{\nu}{D} \quad (1c)$$

; where v_c is the average channel velocity (interstitial velocity). Simulations were carried out at *Pe* numbers between 0.1 and 800, reflecting the experimental practice for van Deemter plots seen in the literature. The flow through the columns was, in all simulations considered, laminar, with Re ranging between 2 x 10^{-4} and 0.8, again reflecting experimental practice. Accordingly, Stokes flow (*Re << 1*) was considered to be present in the system modelled if *Pe* was below 100 (*Re < 0.2*).

2.5. Estimators for column performance

The chromatographic performance of the various packings considered was evaluated and compared in terms of reduced plate height, *h*, dimensionless permeability, *k,* and separation impedance, *E*. A series of simulations were generated at different values of the Peclet number, or reduced velocity. The reduced plate height at various Peclet values was plotted to create van Deemter plots, which are commonly used to determine the conditions for optimal chromatographic performance of a given column [29].

The theoretical plate height values were derived from the simulated RTD profiles. In turn, these were generated as a series of time snapshots of the average concentration at specific transverse cross-sections in the column (Eq. 2).

$$\bar{c}(t)\big|_{z=\tilde{z}} = \frac{\iint_A c(t,x,y)\big|_{z=\tilde{z}}\, v_z(x,y)\big|_{z=\tilde{z}}\, dA}{Au} \quad (2)$$

; where $\bar{c}(t)\big|_{z=\tilde{z}}$ is the average concentration at time t and at the cross-section of generic coordinate $z=\tilde{z}$, $c(t,x,y)\big|_{z=\tilde{z}}$ is the local concentration of the tracer at $z=\tilde{z}$, $v_z(x,y)\big|_{z=\tilde{z}}$ is the local axial velocity at $z=\tilde{z}$, A is the column cross section, $u=\varepsilon v$ is the superficial velocity in the column, and ε is the bed porosity. The method of moments was then applied to the RTD curves to calculate the reduced plate height between two consecutive cross-sections in the column (Eq. 3) [30].

$$h = \frac{\sigma_2^2 - \sigma_1^2}{(t_2 - t_1)^2}\left(\frac{L}{d}\right) \quad (3)$$

; where *t* is the mean residence time of the RTD, σ^2 is the variance of the RTD and *L* is the axial length between the two cross-sections of relevance (subscripts 1 and 2).

The pressure drop per unit length, *dP*/*dz*, was non-dimensionalized into a flow resistance parameter, ϕ, according to Giddings (Eq. 4) [31]:

$$\phi = -\frac{dP}{dz} \cdot \frac{{d_p}^2}{v_c \mu} \quad (4)$$

where μ is the fluid dynamic viscosity. The flow resistance parameter is related to the dimensionless system permeability, k (Eq. 5).

$$k = \frac{\varepsilon}{\phi} = \frac{u\,\mu}{d^2}\frac{1}{-\frac{dP}{dz}} \quad (5)$$

Combining reduced plate height and flow resistance leads to the definition of the separation impedance, E (Eq. 6) [32]:

$$E = h^2\phi \quad (6)$$

The separation impedance is weighted toward plate height because in chromatographic practice this parameter is considered more important than flow resistance alone. Low values for both h and ϕ, and therefore of E, are indicative of good chromatographic efficiency. Accordingly, the minimum impedance, E_{min}, estimated at the minimum reduced plate height, h_{min}, was used to draw comparisons between the different packings.

Finally, tortuosity was employed as a metric to compare identical packing arrangements that differ in their orientation with respect to the main flow direction. Geometric measures of tortuosity are independent of orientation but velocity profiles are not, so we used the definition by Matyka et al. [33], which is the ratio of the sum of total velocity, v_{tot}, to the sum of axial velocity , v_z, across a unit cell. In general, this definition would require an integration of the velocity field over the entire domain. However, thanks to the homogeneous mesh in the LB domain, the summation operator can be employed instead (Eq. 7).

$$T = \frac{\Sigma v_{tot}}{\Sigma v_z} \quad (7)$$

3. Results & Discussion

3.1. Mesh independence tests

Prior research into random packings of homogeneous spheres employed a mesh of $R = 30^3$ nodes per sphere, as reasonable compromise between simulation accuracy and the large number of particles entering the simulation [10, 11, 15]. Mesh independence was also analysed in this work to determine the appropriate number of nodes required to properly describe the spherical particles (Fig. 2). At 30^3 nodes per particle, the error for both plate height and permeability was at most 7% from the reference values measured at a resolution of 90^3. At 50^3 nodes, the error reduced to at most 2.5% from the reference. As the resolution increases, the simulation time increases at a rate proportional to R^5 and the memory requirements increase proportional to R^3 (where R is the system resolution). Considering the computing resources available, we concluded that $R = 30^3$ was a good compromise for reliably solving simulations in a reasonable time.

3.2. Entry Length

The Neumann and Dirichlet boundary conditions selected at the entrance and exit of the packings are

descriptive of a chromatography column with “real” inlet and outlet. This choice had the benefit of enabling us to monitor the flow and concentration profiles at various points within the column, which should provide advantages when extending these models to real adsorption problems. This is an element of novelty with respect to previous work, where periodic boundaries in the axial direction were used [7, 26]. Accordingly, the domain was composed of an appropriate series of unit cells (Fig. 1) aligned in the axial direction. In such domains, a transition from flat velocity profile and fully developed flow occurs in an entrance region downstream of the column inlet [34]. In this work, the entry length was determined by comparing the reduced plate height between two consecutive sampling cross-sections (Eq. 2), and checking if this remained unchanged within 1% for each sampled section thereafter. For ordered packings, the relevant RTD curves were simulated at cross-sections positioned at periodic intervals along the axial length (Fig. 3a). For random packing, cross-sections were located at intervals spaced at the characteristic particle length, i.e. the particle diameter.

For the ordered packings, entry length reduced as bed porosity decreased from SC to BCC to FCC (Fig. 3, Table 1). This result indicates that a more compact bed, with lower degrees of channel-like flow patterns, has the capability to more efficiently disrupt the inlet linear flow profile. This same observation can be made in terms of tortuosity (Fig. 3), where a more tortuous flow pattern favours transverse mixing, thus reducing the entry length. This is particularly apparent with the SC configuration, where the [001] orientation was characterized by a larger entrance region and a lower tortuosity with respect to the [011] and [111] orientations. The entry length was also correlated with Re, where higher velocities required longer entry lengths. At relatively low Re, i.e. close to Stokes flow conditions, all packing types had an entry length of one unit cell. In this case, viscous forces are more relevant than inertial forces, hence favouring the rapid establishment of a fully developed flow profile. Clearly, when outside the Stokes flow regime, the entry length extended beyond the first unit cell. It is worth noting here that the entrance length does not have a significant impact on practical chromatography columns with ordered packing configurations.

Interestingly, the entry length for random packing did not extend beyond the first bead diameter. This is consistent with the tortuous nature of random configurations, where the flat velocity profile is immediately disrupted by the packed bed. Because of variations in the geometry from one sampling section to the following one (a distance of one particle diameter), the reduced plate height and permeability varied markedly between consecutive segments. This problem was overcome by evaluating the key performance indicators as the average between a number of longer sampling sections over five independent random packings.

3.3. Chromatographic performance of sphere packing arrangements

As introduced in Section 2.4, the simulation approach used in this work differed from the methodology used by both Schure et al. [7] and Khirevich [26] in their computational studies on particle packing. First, the previous authors used the Random Walk Particle Tracking (RWPT) method to simulate tracer particles in the porous system and, second, they used periodic boundary conditions to simulate an infinitely long column. Our simulation procedure was therefore first validated by comparing the reduced plate height of close random packing against these previous studies. The van Deemter curves presented in Fig. 4 show that our results were quantitatively consistent with those reported by Khirevich. Although the optimum Peclet number is in agreement with the data reported

by Schure et al., the reduced plate heights in both our work and that of Khirevich are significantly lower. To further validate our approach, we simulated Taylor-Aris dispersion in a cylindrical capillary and found close agreement with the analytical solution (data not shown). The close random packing arrangement of particles is a limiting case, with the minimal bed porosity of 36% reached in chromatographic practice only in extremely well-packed columns. Bed porosity is a key parameter in conventional, randomly packed chromatography columns. For example, packing operations aim to achieve a target porosity of 36–40%, because higher porosities cause loose packing that is prone to channelling and bed non-homogeneities [35]. This practical aspect was validated by Khirevich through computational simulations, showing that, for random packings of monodisperse particles, plate height increases with void fraction [26].

Similar arguments were put forth for ordered packings of monodisperse spheres by Schure at al., who observed an improvement in plate height as the void fraction decreased progressively from SC, BCC and FCC configurations of particles [7]. While this trend is consistent with the behaviour of random packings, such ordered configurations were only investigated in the basic [001] alignment, and the influence of other important packing factors were not considered. In fact, ordered arrangement of particles have a completely different orientational freedom than random packings, defined not only by particle arrangement, but also orientation, shape of particles, and careful combination of appropriately polydisperse particles. To date, the full variety and combinations of ordered packing and their effect on chromatographic performances has not been thoroughly investigated. In turn, no definitive methods or packing parameters are available to help predict the chromatographic performance of an ordered packing of particles. We therefore constructed Van Deemter plots for ordered packings in the range of *Pe* 0.5 to 800 for each configuration and orientation investigated.

In Fig. 5 we show the van Deemter curves for ordered packings in the [001] orientation as well as for random packing. The curves have a characteristic concave upward shape with minimum reduced plate height located in the Peclet region between 5 and 10, except for FCC, which presents its minimum at *Pe* between 20 and 40. In general, FCC [001] produced the lowest h_{min} value, followed by BCC [001] and SC [001]. Compared with ordered packings, random packing displayed the minimum plate height, comparable to the SC [001] configuration, and progressively outperformed SC [001] at around *Pe* = 20, BCC [001] at around *Pe* = 100 and trended to outperform FCC [001] at *Pe* > 1000. In the [001] orientation, the axial flow direction is orthogonal to the standard cubic cell face (Fig. 1). As noted above, the reduced plate height data for ordered sphere packings again differed quantitatively from Schure's initial study, but they are in agreement with a recent study by Li et al [8], who used analytical methods to produce their data (Fig. 6).

Orientation of the ordered packing with respect to the axial direction, i.e. the main direction for fluid flow, is one of the key degrees of freedom that was expected to produce significant changes in the flow patterns. In turn, this should affect the dispersion behaviour within the packing and consequently chromatographic performance. Given the regular structure of the cubic unit cells in ordered packings, only three alignments with respect to the main direction of flow were investigated, namely the [001], [011] and [111] orientations. These constitute principal positions for a regular lattice, and any other transitional alignment would be expected to result in intermediate performance between these limiting cases.

In Fig. 7 we show the van Deemter curves for all the lattice configurations and orientations

considered, while Table 2 summarizes the corresponding minimum plate heights, permeability and separation impedance data. Fig. 7 highlights the apparent influence of lattice orientation on chromatographic performance. All rotations from the [001] orientation reduced the reduced plate heights of both SC and BCC arrangements, while the performance of FCC remained relatively unchanged for the FCC [111] orientation but was impaired in the FCC [011] orientation. Ultimately, FCC [001] displayed the lowest reduced plate height, but other rotated configurations also resulted in comparatively small h_{min}, such as SC [111], BCC [011], BCC [111] and FCC [111]. These results clearly indicate that, while porosity alone may be a sufficient indicator of chromatographic efficiency for random packings, other factors must be considered for ordered packings.

Orientation also has a strong impact on the range of *Pe* at which the reduced height remains close to its minimum. This is most effectively illustrated by the SC series, where SC [001] and SC [011] showed a sharp drop in efficiency as the Peclet number increased above 20, whereas in the case of SC [111], the plate height remained relatively low even at higher reduced velocities. This same behaviour can also be observed for the FCC [111] configuration, endowed with a shallower gradient than FCC [001]. These results indicate that it is possible to operate columns with ordered beds at relatively high velocities without significant loss in performance, with consequent benefits in terms of column throughput, especially in preparative and industrial applications.

Pressure drop across a column is another key factor in chromatographic operations. The relatively low voidage of random beds (36–40%) causes high resistance to flow, thus limiting the operational flow rates, particularly for soft materials subject to deformation and compressibility issues. A similar degree of flow resistance is expected also for the ordered packings, with porosities ranging from 26% for FCC to 48% for SC (Table 1). Table 2 shows that each family of ordered packing shared very similar flow resistance, practically unaffected by orientation with respect to the direction of the flow. Yet, the different particle arrangements were characterized by apparently different permeability values, with the SC being the most permeable and the FCC the configuration with the highest flow resistance. This is consistent with the Carman-Kozeny expression, which postulates that pressure drops depend only on porosity if the fluid (i.e. its viscosity), flow rate (i.e. superficial velocity) and particle size are fixed [36]:

$$\frac{dP}{dz} = -180\,\frac{(1-\varepsilon)^2}{\varepsilon^3}\,\frac{\mu}{d^2}\,u \qquad (8)$$

The Carman-Kozeny expression can be compared with the dimensionless permeability (Eq. 4) to obtain the following relationship:

$$\frac{1}{k} = 180\,\frac{(1-\varepsilon)^2}{\varepsilon^3} \qquad (9)$$

Fig. 8 presents the correlation between the left and the right-hand terms in Eq. 9 for the different packing arrangements considered, where the former term is calculated using the simulated permeability values and the latter using the theoretical bed porosities. The extremely good agreement between simulations and theory is consistent with previously reported system permeabilities for random and [001] ordered packings [7, 37, 38] and provides further confidence in the simulation procedures used in this work.

In terms of separation impedance (Table 2), SC [111] was by far the best performer - with values more than three times lower than that of the second-best arrangement - followed by FCC [001] and BCC [011]. The SC [111] configuration had a h_{min} of 0.16, which is within the range of other high performing configurations (0.10 for FCC [001], 0.19 for BCC [111]). This, coupled with the high permeability of the SC family, explains the exceptional performance of SC [111] in terms of separation impedance. These results suggest that such arrangement would be attractive for use in real chromatographic stationary phases. In addition, practical limitations in 3D printing capabilities, such as the large file size needed to describe the entire internal geometry of the packing [12], and the fidelity of the printed objects [13], are more easily overcome with a looser configuration of particles, making this arrangement a realistic goal in practical manufacturing terms. A potential drawback with SC packing is the physical instability of the bed, wherein the high voidage might cause the particles to move under the influence of physical vibration, thus disrupting the ordered bed arrangement. In AM practice, this drawback can be overcome by slightly overlapping the individual particles to increase the structural stability of the bed [39].

3.4. Influence of tortuosity on chromatographic performance

Low bed voidage has generally been considered critical to ensure good chromatographic performance in randomly packed beds. Approaching the theoretical limit of random close packing is the ideal goal in conventional packed columns because this ensures the absence of channelling or dead zones. The results from our study challenge, for the first time, the concept that excellent chromatographic performance is only possible at low bed porosities. A simple correlation between porosity and reduced plate height does not hold in ordered arrays of spheres, and other parameters and conditions must therefore be taken into consideration. It is possible that these other factors have greater influence on column performance.

The two main dispersion terms in chromatography are associated with the transverse and axial directions [40]. Good transverse dispersion is desirable because it ensures uniform properties over column cross-sections and helps reduce variations in axial velocity associated with defects in the packing [10]. On the other hand, axial dispersion is responsible for band broadening effects and should be kept as low as possible [31]. Coupling of these two parameters finds an analogy in the tortuosity, a metric that describes the axial deviation of the flow paths in a system. In porous media, tortuosity gives an indication of how the flow paths differ, on average, from straight flow channels. Several methods have been proposed to determine the tortuosity of a flow system using the shape of the flow channels. In this study, we used the procedure proposed by Matyka and Koza, in which the tortuosity is computed from the flow field itself, as the ratio between the sum of the magnitudes of the velocity vectors and the sum of their axial components [33]. Here, tortuosity in ordered packing was calculated in a single unit cell after the entrance region, while it was averaged over ten samples of 50^3 simulation nodes in size (approx. $[1.5\ d_p]^3$) on the five independent random packings considered. It was first verified that, for any given packing beyond the entry length, the tortuosity was independent of reduced velocity and column location. This is reasonable as the flow field was always within the laminar regime. The resulting tortuosity values, T, are summarized in Table 2.

Rotation of the regular packings had an appreciable effect on the resulting tortuosity and, in turn, on the fluid flow patterns (Fig. 9). The SC [001] packing, with highest axial dispersion, presented inter-

particle channels mainly extending in the axial direction, with relatively little transverse flow. Packings such as SC [011], BCC [001] and FCC [011] formed packings with channels predominantly oriented in the axial dimension but not both transverse dimensions. These latter packings had lower dispersion than SC [001], but higher than the highest performing configurations, SC [111], BCC [011], BCC [111], FCC [001] and FCC [111], which were characterized by channels actively propagating the flow in all three spatial dimensions. Clearly, a greater number of dimensions in which the inter-particle channels direct the fluid flow correlates to higher transverse mixing and lower band broadening.

This observation is consistent with an inverse relation between tortuosity and minimum reduced plate, shown by the simple linear trendline in Fig. 10. In this tortuosity vs h_{min} plot, the data points for the different configurations were clustered in three main regions, apparently distinguished by the dimensionality of the flow-paths defined by the channels. The SC [001] geometry, endowed with the lowest tortuosity because of its relatively straight channel-like paths, was characterized by the highest h_{min}, indicating the lowest performance in chromatographic applications. In contrast, FCC [001], the configuration with the smallest $h_{\min}$ amongst the geometries investigated, had the highest tortuosity. The other arrangements forming three-dimensional channels also performed comparatively well. The trend shown here offers a strong clue for directing further research efforts into the design of ordered packings for chromatography. It is reasonable to expect that the inverse correlation shown here for the ordered packings of monodisperse spherical particles will also hold for other types of ordered packings, with improved geometries characterized by higher tortuosity factors. For example, improved chromatographic beds could comprise polydisperse spheres with particles of appropriate dimensions and a suitable 3D arrangement [41] or the use of ellipsoids with the major axes aligned in the transverse directions, similar to the trapezoidal pillars proposed in 2D chromatography [42]. Beds with the greatest performance might not even be composed of particles at all, but might rather be monolithic, comprising a tortuous lattice of appropriately designed channels that improve radial dispersion while limiting axial band broadening.

Interestingly, random packing did not follow the trend observed for the ordered packings, having a relatively large reduced plate height despite its high tortuosity. We suspect this inefficiency stems from the greater eddy dispersion present in random packings. Eddy dispersion is closely related to the 'A' term in van Deemter's plate height equation and is also linked to the wide distribution of path lengths within a porous medium [29]. This observation again demonstrates that the performance of random beds is, in general, inferior to that of ordered packings.

4. Conclusions

In this work, the LBM model was used to simulate the flow and extra-particle mass transfer properties within ordered and random arrangements of non-porous, monodisperse spherical particles. The approach taken, including the initial and boundary conditions, was analogous to practical experimental systems, offering a new tool for the CFD simulation of real chromatographic columns. Although ordered lattices of particles have been, prior to now, regarded as purely hypothetical propositions, the emergence of additive manufacturing methods offer the potential to manufacture complex 3D objects, thus changing the context of porous media design to one of industrial relevance.

CFD can therefore serve as a basis to design, *a priori*, porous stationary phases for chromatography columns with improved geometries, which can then be manufactured using AM.

Several packing geometries were discussed in terms of reduced plate height, permeability, separation impedance, and tortuosity. The influence of the orientation of the ordered beds with respect to the main direction of flow was evaluated, a novel concept not previously considered in ordered packings. While the orientation of the packing has no effect in randomly packed beds, we propose that the alignment of the packing with respect to the bulk flow offers a new consideration in ordered packing design. We found a linear inverse relationship between tortuosity and minimum reduced plate height for the ordered packings investigated, demonstrating that ordered packings characterized by higher tortuosity promote transverse mixing while reducing axial dispersion. However, bed permeability depends mainly upon the porosity of the bed (for a given characteristic dimension of the spherical particles), so the pressure drop across beds with same packing arrangement is virtually independent of tortuosity. Thus, appropriate rotation of the lattice results in a stationary phase with higher tortuosity and smaller reduced plate height but without a concurrent increase in pressure drop, effectively leading to improved chromatographic performance in terms of minimum separation impedance. This behaviour was particularly strong for the SC [111] configuration, which achieved the lowest separation impedance amongst the simulated packings studied because it has a relatively loose structure (48% bed porosity, leading to low pressure drops), and a low plate height (because of the high tortuosity of its internal flow paths). An increase in throughput is also expected by the practically negligible impact of higher flow rates on plate height, as observed in the FCC [001] and FCC [111] configurations.

The use of low-dispersion stationary phases with low pressure drop characteristics has wide potential for applications beyond chromatography involving porous media, such as in water purification, regenerative medicine, drug delivery, and catalysis. We also expect that these results can be extended beyond ordered lattices of monodisperse spheres, comprising particles with different shapes, sizes and relative alignments or monolithic structures composed of ordered networks of appropriately sized and interconnected channels.

Acknowledgements

This work was supported by funding from the Ministry of Business, Innovation and Employment (MBIE) of New Zealand (UOCX14 and UOCX15) and help and support from the New Zealand eScience Infrastructure (NeSI), Francois Bissey and Daniel Lavagra, formerly of the BlueFern HPC team at the University of Canterbury. The authors are grateful to Jonas Latt and Dimitrios Kontaxakis of FlowKit Ltd. (Lausanne, Switzerland) for support during the implementation of Palabos.

References

1. Ganetsos, G. and P.E. Barker, *Preparative and production scale chromatography*. Vol. 61. 1992: CRC Press.
2. Macek, K., Z. Deyl, and J. Janák, *Liquid Column Chromatography: A Survey of Modern Techniques and Applications*. Vol. 3. 2011: Elsevier.
3. Lough, W.J. and I.W. Wainer, *High Performance Liquid Chromatography: Fundamental Principles and Practice*. 1995: Taylor & Francis.
4. Heftmann, E., *Chromatography: Fundamentals and applications of chromatography and related differential migration methods - Part A: Fundamentals and techniques*. 2004: Elsevier Science.
5. Natarajan, V., Mann, Anthony Frederick, Schubnel, Daniel, *Method of and Device for packing a Chromatography Column*. 2015, EMD Millipore Corporation: United States.
6. Schmidt-Traub, H., M. Schulte, and A. Seidel-Morgenstern, *Preparative Chromatography*. 2012, Hoboken, New Jersey, USA: Wiley.
7. Schure, M.R., R.S. Maier, D.M. Kroll, and H. Ted Davis, *Simulation of ordered packed beds in chromatography.* Journal of Chromatography A, 2004. **1031**(1–2): p. 79-86.
8. Li, L., X. Yan, J. Yang, and Q. Wang, *Numerical investigation on band-broadening characteristics of an ordered packed bed with novel particles.* Applied energy, 2017. **185**: p. 2168-2180.
9. Li, L., X. Yan, J. Yang, and Q. Wang, *Computational Study of Chromatography Performance in Ordered Packed Beds with Spherical or Ellipsoidal Particles.* Energy Procedia, 2015. **75**: p. 3322-3327.
10. Daneyko, A., D. Hlushkou, S. Khirevich, and U. Tallarek, *From random sphere packings to regular pillar arrays: Analysis of transverse dispersion.* Journal of Chromatography A, 2012. **1257**: p. 98-115.
11. Daneyko, A., S. Khirevich, A. Höltzel, A. Seidel-Morgenstern, and U. Tallarek, *From random sphere packings to regular pillar arrays: Effect of the macroscopic confinement on hydrodynamic dispersion.* Journal of Chromatography A, 2011. **1218**(45): p. 8231-8248.
12. Fee, C., S. Nawada, and S. Dimartino, *3D printed porous media columns with fine control of column packing morphology.* Journal of Chromatography A, 2014. **1333**: p. 18.
13. Nawada, S., S. Dimartino, and C. Fee, *Dispersion behavior of 3D-printed columns with homogeneous microstructures comprising differing element shapes.* Chemical Engineering Science, 2017. **164**: p. 90-98.
14. Vangelooven, J. and G. Desmet, *Theoretical optimisation of the side-wall of micropillar array columns using computational fluid dynamics.* Journal of Chromatography A, 2010. **1217**(52): p. 8121-8126.
15. Schure, M.R., R.S. Maier, D.M. Kroll, and H.T. Davis, *Simulation of Packed-Bed Chromatography Utilizing High-Resolution Flow Fields: Comparison with Models.* Analytical Chemistry, 2002. **74**(23): p. 6006-6016.
16. Succi, S., *The Lattice Boltzmann Equation: For Fluid Dynamics and Beyond*. 2001: Clarendon Press.
17. Guo, Z. and C. Shu, *Lattice Boltzmann Method and Its Applications in Engineering*. 2013: World Scientific Publishing Company.
18. FlowKit Ltd. (2011). *Parallelism*. Retrieved 20 May 2017 from http://www.palabos.org/.
19. Krüger, T., H. Kusumaatmaja, A. Kuzmin, O. Shardt, G. Silva, and E.M. Viggen, *The Lattice Boltzmann Method: Principles and Practice*. 2016: Springer International Publishing.
20. Solidscape Inc. (2017). *3D Printers*. Retrieved 30 June 2017 from http://www.solid-scape.com/.
21. Baranau, V. and U. Tallarek, *Random-close packing limits for monodisperse and polydisperse hard spheres.* Soft Matter, 2014. **10**(21): p. 3826-3841.
22. Majid Hassanizadeh, S. and A. Leijnse, *A non-linear theory of high-concentration-gradient dispersion in porous media.* Advances in Water Resources, 1995. **18**(4): p. 203-215.
23. Dai, Q. and L. Yang, *LBM numerical study on oscillating flow and heat transfer in porous media.* Applied Thermal Engineering, 2013. **54**(1): p. 16-25.
24. Bhatnagar, P.L., E.P. Gross, and M. Krook, *A Model for Collision Processes in Gases. I. Small Amplitude Processes in Charged and Neutral One-Component Systems.* Physical Review, 1954. **94**(3): p. 511-525.
25. Perko, J. and R.A. Patel, *Single-relaxation-time lattice Boltzmann scheme for advection-diffusion problems with large diffusion-coefficient heterogeneities and high-advection transport.* Physical Review E, 2014. **89**(5): p. 053309.
26. Khirevich, S., *High-Performance Computing of Flow, Diffusion, and Hydrodynamic Dispersion in Random Sphere Packings*, in *Department of Chemistry*. 2010, Philipps-Universität Marburg.
27. Crittenden, J.C., H. Montgomery Watson, and I. Books24x, *MWH's water treatment: principles and design, third edition*. 3rd ed. 2012, Hoboken, New Jersey, USA: John Wiley & Sons.
28. Haynes, W.M., *CRC Handbook of Chemistry and Physics, 97th Edition*. 2016, Boca Raton, Florida, USA: CRC Press.

29. van Deemter, J.J., F.J. Zuiderweg, and A. Klinkenberg, *Longitudinal diffusion and resistance to mass transfer as causes of nonideality in chromatography.* Chemical Engineering Science, 1995. **50**(24): p. 3869-3882.
30. Levenspiel, O., *Chemical reaction engineering*. 3rd ed. 1999, Hoboken, New Jersey, USA: John Wiley & Sons.
31. Giddings, J.C., *Dynamics of Chromatography: Principles and Theory*. 2002: Taylor & Francis.
32. Poole, C.F., *The Essence of Chromatography*. 2003: Elsevier.
33. Matyka, M., Z. Koza, and K. Vafai. *How to calculate tortuosity easily?* in *AIP Conference Proceedings 4*. 2012. AIP.
34. Bird, R.B., W.E. Stewart, and E.N. Lightfoot, *Transport phenomena*. 2007, Hoboken, New Jersey, USA: John Wiley & Sons.
35. Carta, G. and A. Jungbauer, *Protein chromatography: Process Development and Scale-up*. 2010, Hoboken, New Jersey, USA: John Wiley & Sons.
36. Pohorecki, R., J. Bridgwater, and M.M.R.G.C. Gallegos, *Chemical Engineering and Chemical Process Technology - Volume II: Unit Operations – Fluids and Solids*. 2010, Paris, France: EOLSS Publications.
37. Sangani, A.S. and A. Acrivos, *Slow flow through a periodic array of spheres.* International Journal of Multiphase Flow, 1982. **8**(4): p. 343-360.
38. Zick, A.A. and G.M. Homsy, *Stokes flow through periodic arrays of spheres.* Journal of Fluid Mechanics, 2006. **115**: p. 13-26.
39. Nawada, S., S. Dimartino, and C.J. Fee, *The Effects of bead overlap on chromatographic performance in 3D printed packed bed columns.* International Labmate, 2014.
40. Tallarek, U., K. Albert, E. Bayer, and G. Guiochon, *Measurement of transverse and axial apparent dispersion coefficients in packed beds.* AIChE Journal, 1996. **42**(11): p. 3041-3054.
41. O'Toole, P.I. and T.S. Hudson, *New High-Density Packings of Similarly Sized Binary Spheres.* The Journal of Physical Chemistry C, 2011. **115**(39): p. 19037-19040.
42. Desmet, G., M. Callewaert, H. Ottevaere, and W. De Malsche, *Merging Open-Tubular and Packed Bed Liquid Chromatography.* Analytical Chemistry, 2015. **87**(14): p. 7382-7388.

List of Figures

Figure 1. Visualization of packing: a) SC [001], b) SC [011], c) SC [111], d) BCC [001], e) BCC [011], f) BCC [111], g) FCC [001], h) FCC [011], i) FCC [111] and j) Random Packing. The main direction of the flow is in the z axis.

Figure 2. Mesh independence investigation for a) permeability and b) reduced plate height for crystal cubic packing of spheres. k_{90} *and* h_{90} *represent the permeability and plate height values measured at the reference* 90^3 *mesh.*

Figure 3. a) Illustration of the method used to calculate the height equivalent of a theoretical plate between two sampling slices, and entry length for ordered sphere packings: b) [001] orientation, c) [011] orientation and d) [111] orientation.

Figure 4. Comparison of data for reduced plate height of jammed close random sphere packing: Schure et al. (blue) [7], Khirevich [25] (red) and this work (green).

Figure 5. van Deemter plots of ordered sphere packings in the [001] orientation, and of jammed randomly packed spheres: a) over the entire simulated Peclet range and b) focused on the minima of each curve.

Figure 6. Comparison of data for reduced plate height of ordered sphere packing in the [001] orientation between Li et. al [8] and this work.

Figure 7. van Deemter plots for each family of packing at different orientations with respect to the main flow direction: a) SC, b) BCC and c) FCC.

Figure 8. Comparison of the reciprocal of the permeability from the LBM simulations (LHS of Eq. 9) and theoretically derived porosity term (RHS of Eq. 9). The diagonal is shown to help visualize the agreement between simulation results and theory.

Figure 9. Representative stream lines of a produced by unit cells of: a) SC [001], b) SC [011], c) SC [111], d) BCC [001], e) BCC [011], f) BCC [111], g) FCC [001], h) FCC [011], i) FCC [111] unit cells. The [001] and [011] have symmetrical channels reflected by yz face (in the positive x direction) while the [111] orientations show the whole unit cell. The normalized velocity is respective to each plot individually. The packing of each unit cell is only shown for the bottom half so that streamlines may be clearly viewed.

Figure 10. Correlation between minimum reduced plate height and tortuosity in the ordered packings considered: SC in blue, BCC in red, and FCC in green. Random packing is also shown, in black.

672

Figure 1

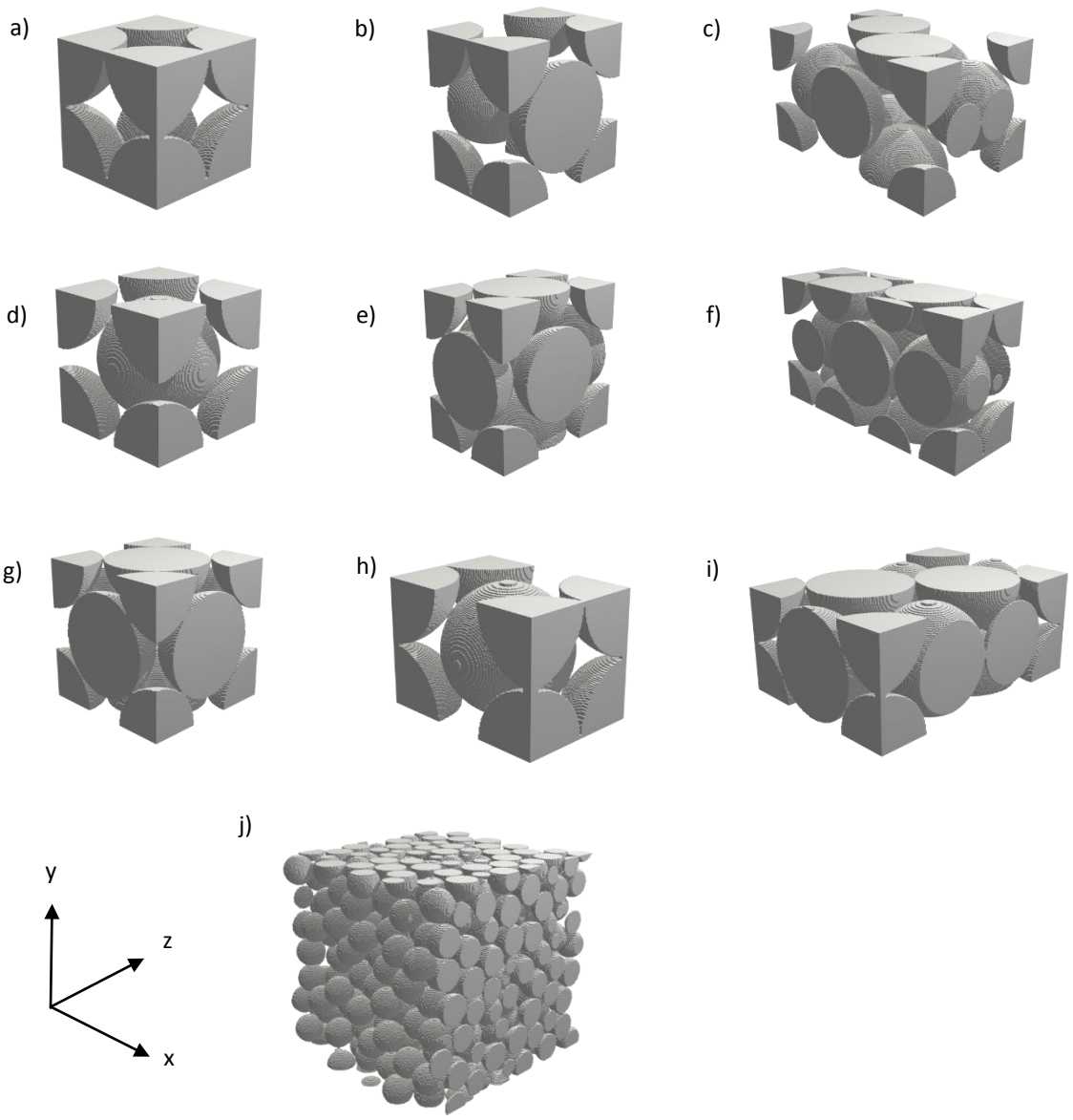

Figure 2

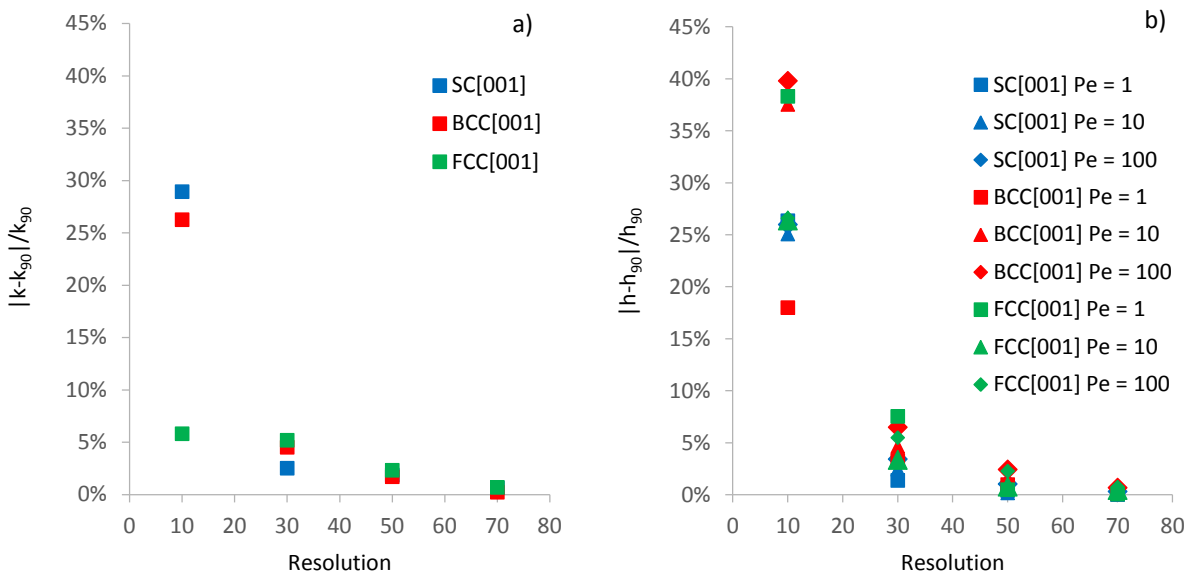
a)
45%
40%
35%
30%
25%
20%
15%
10%
5%
0%
0
10
20
30
40
50
60
70
80
Resolution
|k-k90|/k90
SC[001]
BCC[001]
FCC[001]
b)
|h-h90|/h90
SC[001] Pe = 1
SC[001] Pe = 10
SC[001] Pe = 100
BCC[001] Pe = 1
BCC[001] Pe = 10
BCC[001] Pe = 100
FCC[001] Pe = 1
FCC[001] Pe = 10
FCC[001] Pe = 100

Figure 3

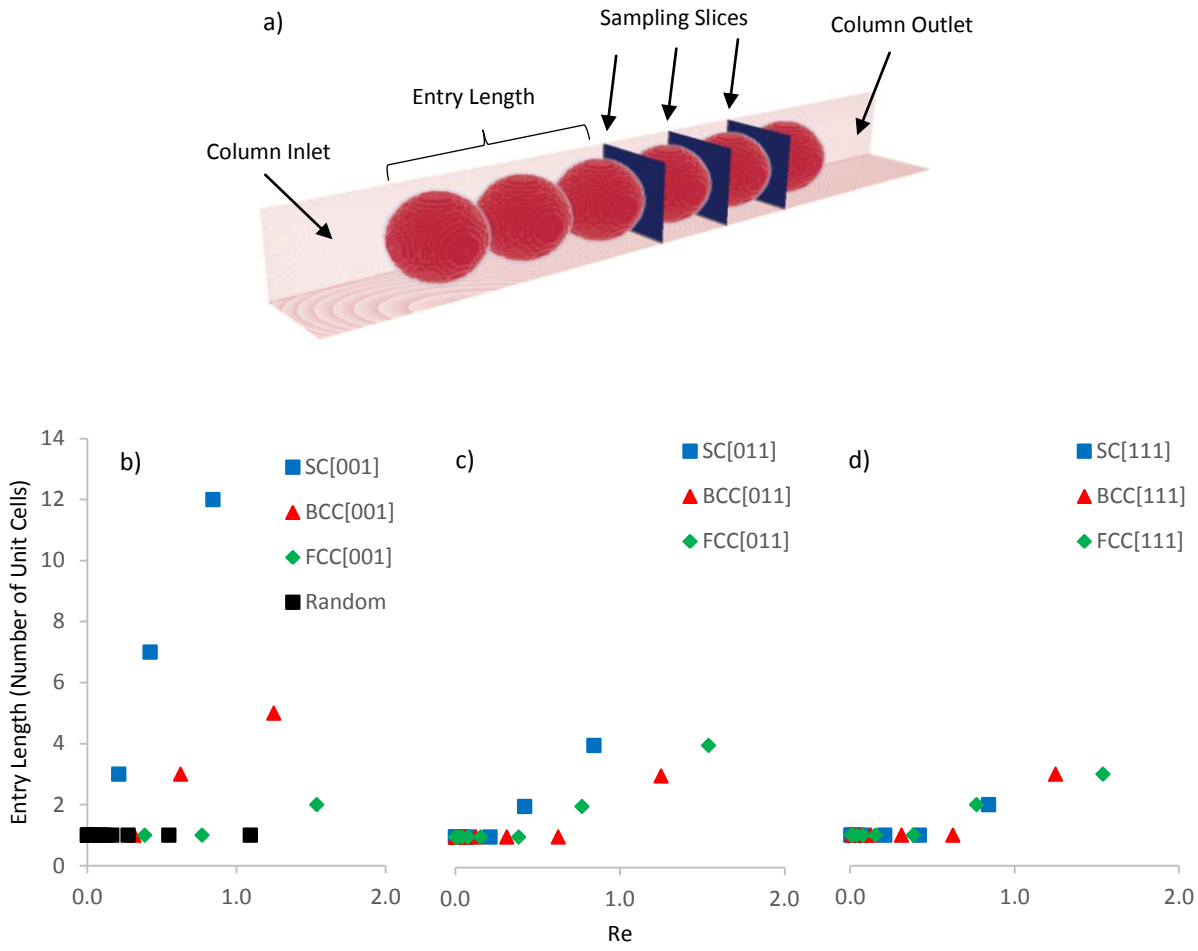
a)
Sampling Slices
Column Outlet
Entry Length
Column Inlet
b)
c)
d)
SC[001]
BCC[001]
FCC[001]
Random
SC[011]
BCC[011]
FCC[011]
SC[111]
BCC[111]
FCC[111]
Entry Length (Number of Unit Cells)
Re
0
2
4
6
8
10
12
14
0.0
1.0
2.0

Figure 4

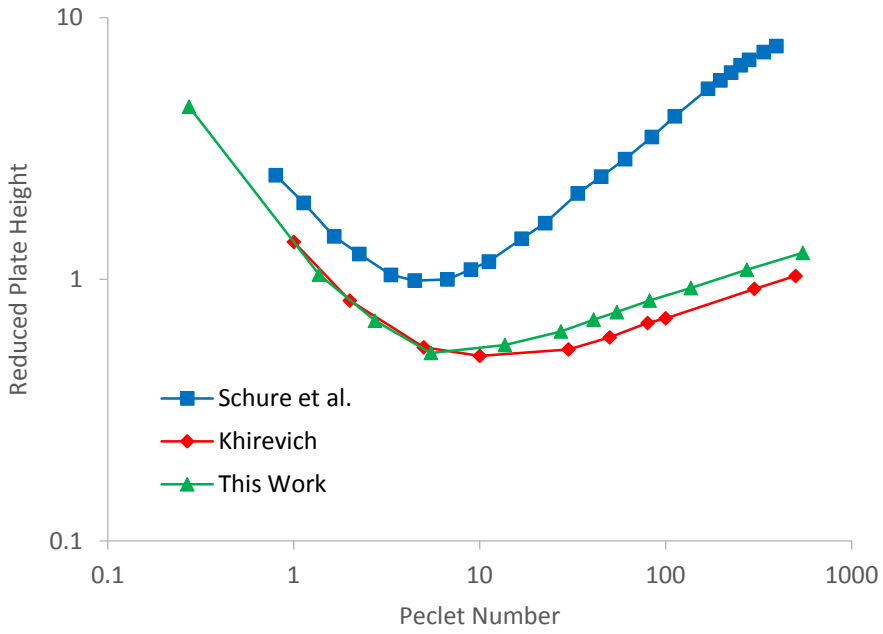
10
1
0.1
Reduced Plate Height
0.1
1
10
100
1000
Peclet Number
Schure et al.
Khirevich
This Work

Figure 5

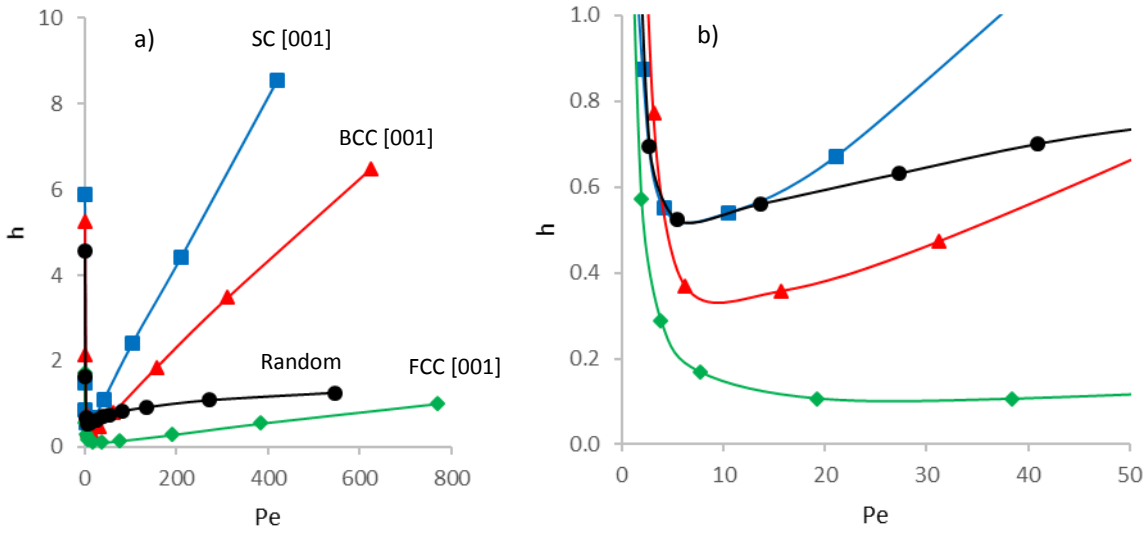
a)
SC [001]
BCC [001]
Random
FCC [001]
h
Pe
10
8
6
4
2
0
0
200
400
600
800
b)
h
Pe
1.0
0.8
0.6
0.4
0.2
0.0
0
10
20
30
40
50

Figure 6

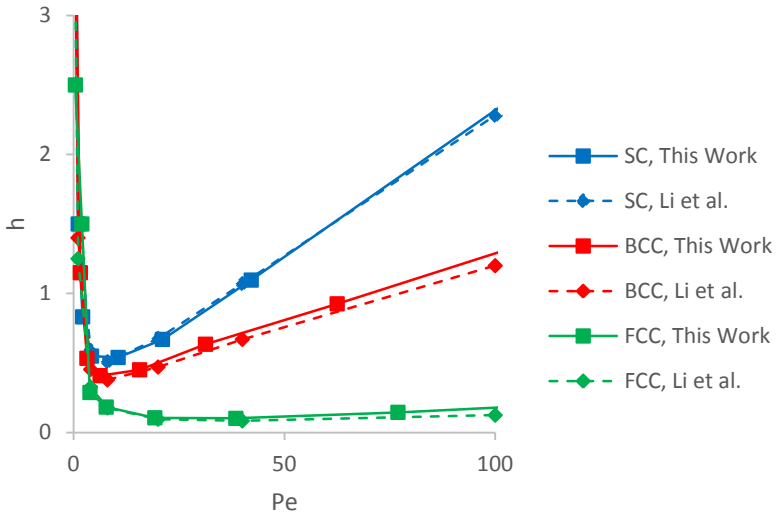
3
2
1
0
h
0
50
100
Pe
SC, This Work
SC, Li et al.
BCC, This Work
BCC, Li et al.
FCC, This Work
FCC, Li et al.

Figure 7

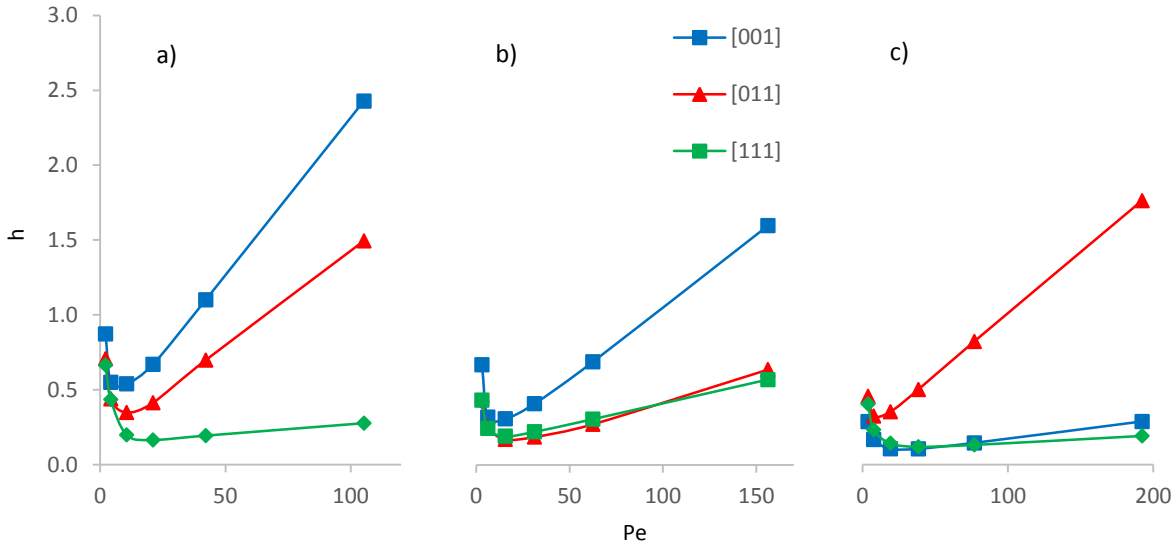

Figure 8

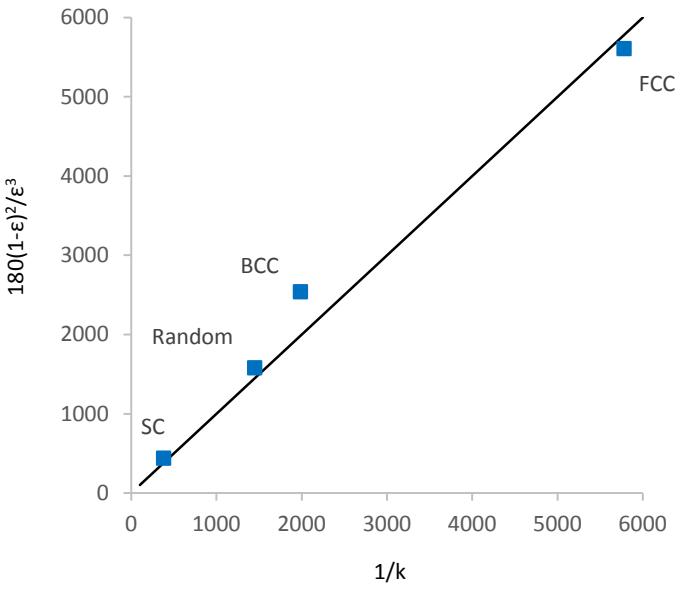
6000
5000
4000
3000
2000
1000
0
180(1-ε)²/ε³
0
1000
2000
3000
4000
5000
6000
1/k
FCC
BCC
Random
SC

Figure 9

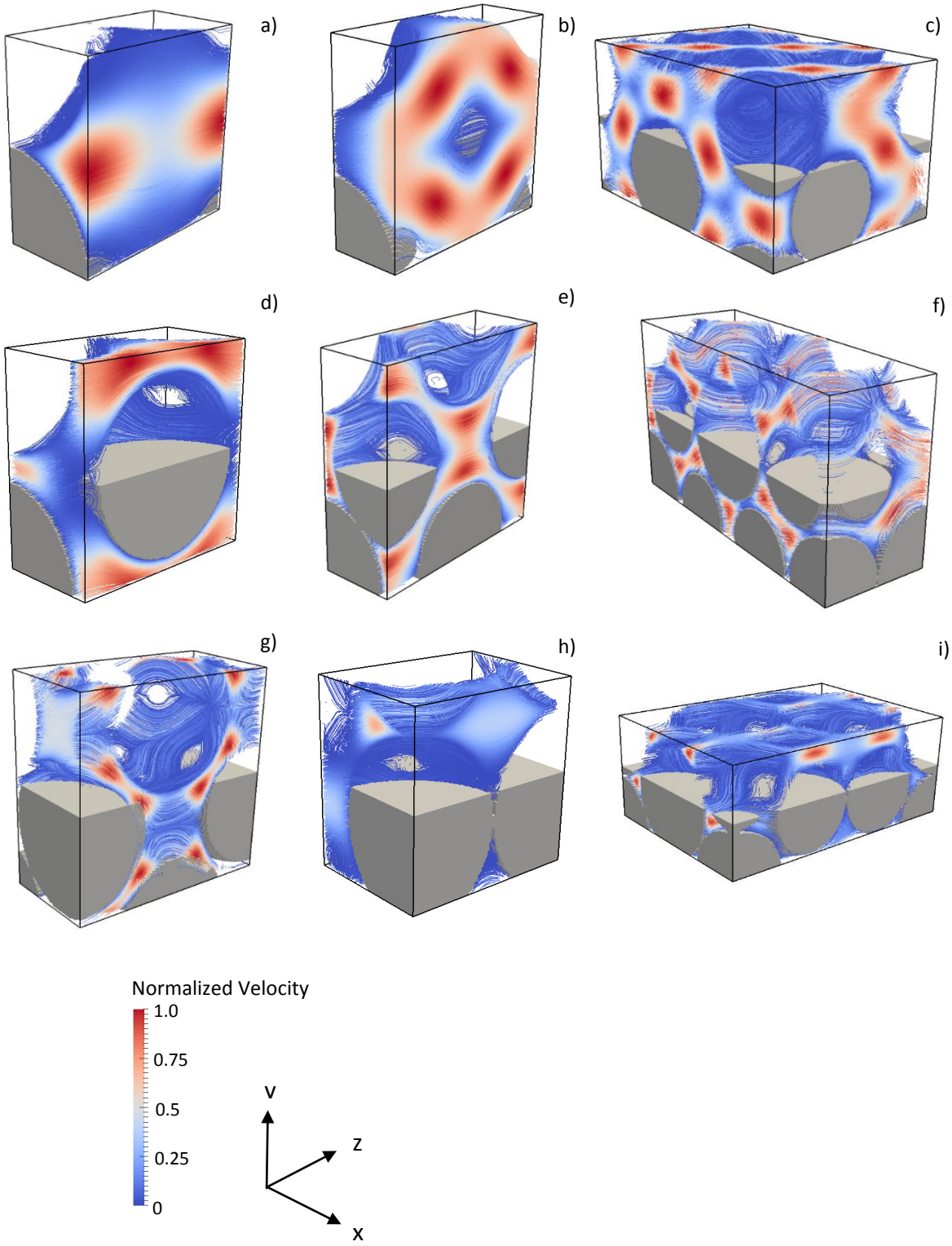

Figure 10

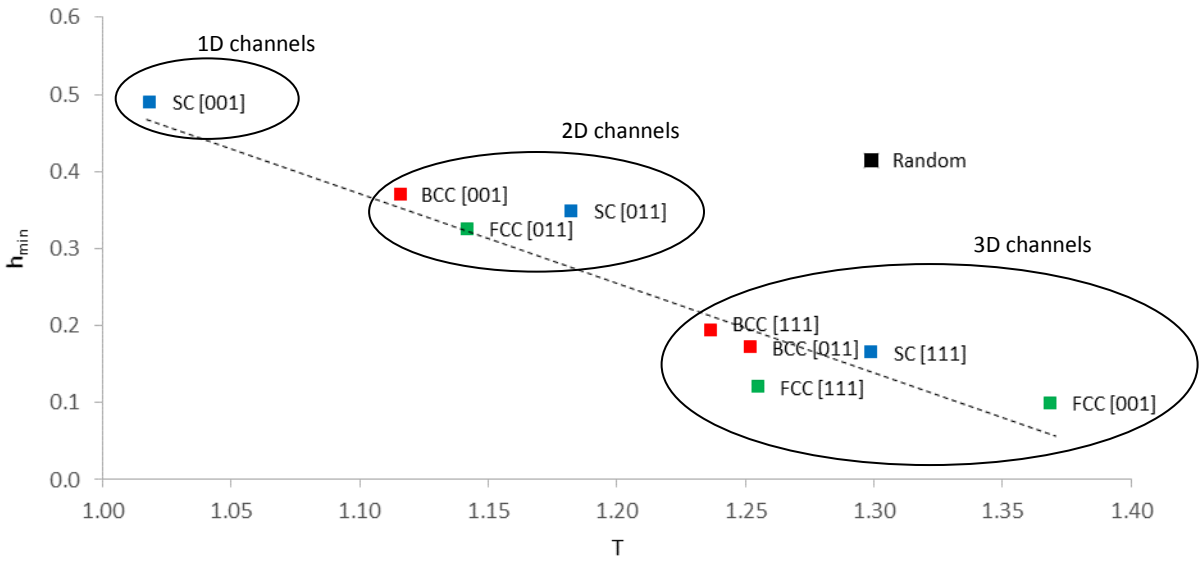
0.6
0.5
0.4
0.3
0.2
0.1
0.0
h_{min}
1.00
1.05
1.10
1.15
1.20
1.25
1.30
1.35
1.40
T
1D channels
SC [001]
2D channels
BCC [001]
SC [011]
FCC [011]
Random
3D channels
BCC [111]
BCC [011]
SC [111]
FCC [111]
FCC [001]

Table 1

Table 1. Unit cell properties of the packings studied.

Packing Configuration	Cell Length[a] (x, y, z)	Particles per unit cell	Porosity
SC [001]	1, 1, 1	1	
SC [011]	1, √2, √2	2	0.48
SC [111]	2√3/√2, √2, √3	6	
BCC [001]	2/√3, 2/√3, 2/√3	2	
BCC [011]	2/√3, 2√2/√3, 2√2/√3	4	0.32
BCC [111]	2√2, 2√2/√3, 1	6	
FCC [001]	√2, √2, √2	4	
FCC [011]	√2, 1, 1	2	0.26
FCC [111]	√3, 1, 2√3/√2	6	
Random	7, 7, 7	416	0.36

[a] Dimensionless length, 1 corresponds to one particle diameter.

Table 2

Table 2. Simulated properties of the packings studied.

Packing Configuration	h_{min}	k	E_{min} [a]	T
SC [001]	0.54	2.64E-03	53	1.02
SC [011]	0.35	2.63E-03	22	1.18
SC [111]	0.16	2.60E-03	5	1.30
BCC [001]	0.36	5.04E-04	81	1.12
BCC [011]	0.17	5.04E-04	19	1.25
BCC [111]	0.19	5.02E-04	24	1.24
FCC [001]	0.10	1.73E-04	17	1.37
FCC [011]	0.33	1.71E-04	161	1.14
FCC [111]	0.12	1.72E-04	22	1.25
Random	0.52	6.91E-04	145	1.30

[a] Separation impedance is estimated at h_{min}.